Reactive and Functional Polymers 148 (2020) 104483

Contents lists available at ScienceDirect

Reactive and Functional Polymers

journal homepage: www.elsevier.com/locate/react

Increased power conversion efficiency of dye-sensitized solar cells with counter electrodes based on porous polypyrrole

Shahzad Ahmad Khan[a,*], Ligui Li[a,*], Dengke Zhao[a], Shaowei Chen[a,b]

[a] Guangzhou Key Laboratory for Surface Chemistry of Energy Materials, New Energy Research Institute, School of Environment and Energy, South China University of Technology, Guangzhou Higher Education Mega Center, Guangzhou 510006, China

[b] Department of Chemistry and Biochemistry, University of California, 1156 High Street, Santa Cruz, California 95064, USA

ARTICLE INFO

Keywords:
Solar energy materials
Porous materials
Polymer film
Simple hydrothermal method

ABSTRACT

The porous polypyrrole (PPPy) was synthesized with zeolitic imidazolate framework-8 (ZIF-8) used as template by simple hydrothermal. The resultant PPPy was employed as counter electrode (CE) in dye-sensitized solar cell (DSSC). The 5% $Cu(ClO_4)_2$ and 2% ZIF-8 ratio in PPPy at 100 °C by simple hydrothermal method demonstrates comparable performance with traditional Pt in DSSC as CE, 8.63% and 9.05% energy conversion efficiency (η), respectively. The electrochemical and photo-electrochemical as well as impedance spectra measurements revealed that ZIF-8 as template by simple hydrothermal method is a effective way for preparing PPPy at 100 °C as CE in DSSC, which may open up an alternative choice for the future industrial application. In DSSC, PPPy at 100 °C is one of the most promising material used for nano-porous thin film when, it serves as CE due to its appropriate low cost, and easy preparation method. The template polymerization of PPPy on zeolytes is interesting method for DSSC and as electro-catalyst, it can be big perspective in polymer membrane fuel cells, Zn air battery, Li ion battery and also useful for hydrogen production from water. So, this article will broaden the application of conductive polymers in DSSCs as well as above described fields.

1. Introduction

The dye-sensitized solar cell (DSSC) is a device to directly convert the solar energy to electric power and has been widely investigated due to its low cost, simple fabrication process and high energy conversion efficiency [1]. A typical DSSC consists of a nano-porous TiO_2 film adsorbed with dye, an iodide/tri-iodide redox electrolyte, and a counter electrode (CE). The CE plays an important role in DSSC especially in terms of energy conversion efficiency. Although commonly used Pt (CE) has high catalytic activity for tri-iodide reduction, it is a rare metal on earth and very expensive, which limits the large-scale production of DSSC. Therefore, cheap and efficient alternative materials have been intensively developed to replace Pt recently, such as carbon materials (graphite, carbon black, activated carbon, carbon nanotube, carbon dye, and fullerene) [2–7], conducting polymers (PEDOT, polypyrrole, polyaniline) [8–13], and vary recently metallic compounds (metal carbides, metal nitrides, and metal sulfides) [14–19]. The polypyrrole (PPy) has received considerable interest due to its excellent chemical stability, conductivity and biocompatibility [20]. It can be easily synthesized at a reasonable cost by a wet method such as a chemical oxidation method [21–23]. The PPy suffers from some issues such as brittle, insoluble and infusible properties due to its rigid conjugated backbone structure. These properties have made it challenging to produce solution and melt processing of the synthesized materials [24]. The conductivity of the materials degrades over time or by the environment, *i.e* ageing [25]. The zeolite, an alumino-silicates microporous material with three-dimensional frameworks, is considered as a good candidate for this task [26]. The acidity of the zeolite surface offers excellent adhesion between the two materials, *i.e.* conducting polymer and zeolite and this result in a combination of fast electronic mobility of the conducting polymer with a possibility of accommodating exchangeable cations of the zeolite to the conducting polymer structure [27]. Few ionic functional groups of the zeolite may act as dopants in the host conducting polymer matrix during synthesis process that will control its electrical property which is essential for electronic and photonic applications [28,29]. So, the conducting polymer/zeolite composite is expected to exhibit improved electrical, thermal, mechanical and sensing properties [30]. This is because of its structure that comprises of pores, channel and cages with different shapes and dimensions in the nanometer scale which makes it a promising host for conducting polymer chain. For this purpose we choose simple hydrothermal method as it shows promising features due to its unique

* Corresponding authors.
E-mail addresses: shahzad.khan2007@yahoo.com (S.A. Khan), esguili@scut.edu.cn (L. Li).

https://doi.org/10.1016/j.reactfunctpolym.2020.104483
Received 10 October 2019; Received in revised form 5 January 2020; Accepted 6 January 2020
Available online 07 January 2020
1381-5148/

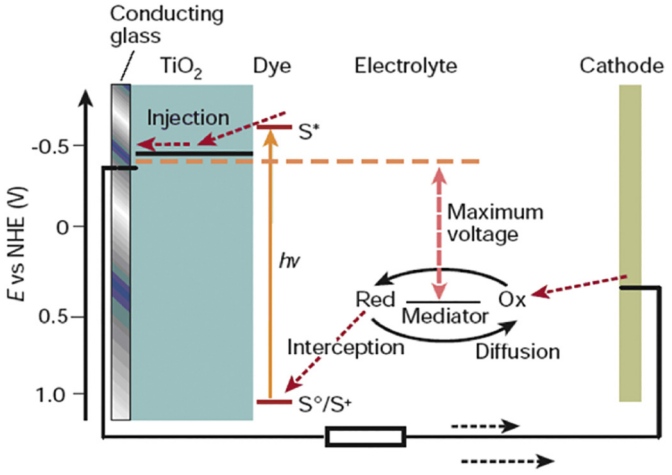

Fig. 1. Schematic representation of the working principle of DSSCs.

synthesis condition, environmental friendly, versatile method and may have promising future in industry. The working principle of DSSCs is not similar to conventional solar cell, but it is similar to natural photosynthesis process where light absorption and charge carrier transportation have different substances, as shown in Fig. 1.

Research into the area of porous polymers has been of great interest for a long time due to their potential applications such as antistatic paints, electro-chromic devices, electrochemical capacitors, biosensors, polymer solar cells (PSCs) and polymer light-emitting diodes (PLEDs). Highly ordered, crystalline materials containing pores are perfect for use in these applications. So, it was needed to work on pyrrole with MOFs as pyrrole with inorganic and organic material already studied. In this work PPPy was synthesized at different temperatures with pyrrole, $Cu(ClO_4)_2$ and ZIF-8 by simple hydrothermal method. The performance of PPPy as CE for DSSC and detailed optimization procedures were investigated.

2. Materials and method

2.1. Synthesis of porous polypyrrole (PPPy)

The pyrrole monomer (Merck) used for the present study was purified by a vacuum distillation before using and others chemicals were purchased from Shenshi Chemical, Ltd. (Wuhan) and used as received. The ZIF-8 nano-crystals in methanol were synthesized according to the route reported by Cravillon et al., [31]. All the chemicals were used without further purification. Firstly, pyrrole monomer with different ratios of compounds like ZIF-8 (2%), oxidizing agent copper(II) perchlorate $Cu(ClO_4)_2{\cdot}6H_2O$ (5%) and butanol solution (30%) were transferred into 100 mL Teflon-Line Autoclave followed by sealing, maintaining at 40 °C for 48 h and naturally cooling down to room temperature. After, heating get the darker yellow slurry mixed it with film-forming agent polyethylene glycol 400 (PEG400 15 wt%) for optimization and pasted on a FTO (Nippon Sheet Glass, SnO_2: F, 14 Ω sq.$^{-1}$) substrate by doctor-blade techniques and incubated at 60–120 °C for 4 h to finish polymerization as seen from the color change from yellow over green to brownish black. Then FTO substrate was washed in methanol and ethanol mixture (with volume ratio 1:1) and FTO was put overnight into the aqueous hydrochloride (HCl) solution (pH = 4) to remove ZIF-8 from PPPy. After, that FTO was dried in vacuum at 90 °C to remove HCl from PPPy and corresponding polypyrrole (CPPy) at 100 °C was synthesized without ZIF-8 as mentioned above procedure. The procedure of PPPy synthesis by simple hydrothermal method was shown in Fig. 2.

2.2. Assembling of DSSCs

The nano-porous TiO_2 electrodes were prepared on a FTO (Nippon Sheet Glass, SnO_2: F, 14 Ω sq.$^{-1}$) from the colloidal Nanoxide-T paste (Solaronix) by doctor-blade techniques. The films were annealed at 450 °C for 30 min in the air. The resulting TiO_2 films (thickness is around 5.5 μm, measured by a profiler, Sloan, Dektak3) were cut into pieces. Then, the electrodes were immersed into 3.0 × 10^{-4} M *cis*-bis (isothiocyanato)(2,2′-bipyridyl-4,4′-dicarboxylato)(2,2′- bipyridyl-4,4′-dinonyl) ruthenium(II) (known as N-719 dye, Solaronix, Switzerland) in a mixture of acetonitrile and tertiary butyl alcohol (with volume ratio 1:1), and maintained at room temperature for 18 h to complete the sensitizer uptake. The dye-sensitized electrode was then washed with ethanol to remove unanchored dye before to use. The organic liquid electrolyte composed of 0.5 M tert-4-butylpyridine, 0.1 M LiI, 0.05 M I_2 and 0.3 M 1,2-dimethyl-3-propylimidazolium iodide in 3-methoxy-propionitrile/acetonitrile (with volume ratio 1:1) was employed for DSSC. The performance evaluation of the DSSC was studied by recording the current-voltage (I-V) characteristics of the unsealed type cell under illumination of AM1.5 (1 Sun; 100 mW cm^{-2}) using a solar simulator (Oriel, 91,167).

2.3. Measurement and characterization

The morphologies and size of different samples were characterized by field emission scanning electron microscopy (FESEM, Hitachi S-4800, Japan). The phase of the samples was analyzed by X-ray powder diffraction (XRD, Rigaku Ultima II, Japan) and absorption spectra measurements were performed with a Shimadzu UV-3600 UV-VIS spectrophotometer in the wavelength 300 to 800 nm. The surface area (BET) was analyzed by NOVA 4200e Surface Area & Pore Size Analyzer. The iodide species of different PPPy or Pt (CE) in DSSCs, was carried out in three electrode measurements in 10 mM LiI, 1 mM I_2 and 0.1 M $LiClO_4$ in acetonitrile. A 1 cm^2 area of PPPy/FTO and Pt/FTO served as working electrodes. A platinum foil and Ag/AgCl served as the counter electrode and the reference electrode (CHI-604D electrochemical system), respectively. The electrical impedance spectra (EIS) was recorded (CHI-604D) over a frequency range of 0.1–10^6 Hz in dark at 25 °C. The ac amplitude and the applied voltage were 10 mV and set −700 mV of the cells, respectively.

3. Results and discussion

3.1. Surface morphologies of various counter electrodes

The Fig. 3, presents a set of typical field emission scanning electron microscopy (FESEM) images of the CPPy (a), PPPy at 60 °C (b), PPPy at 80 °C (c), PPPy at 100 °C (d), PPPy at 120 °C (e), under a strong ultrasonic wave treatment for 1 h, have different morphologies obtained by simple hydrothermal method. The physical properties, morphology and electro-chemical characteristics of PPPy was greatly influenced by the oxidizing reagent and ZIF-8 used as template for polymerization. The particles of pure phase CPPy formed were found to be with particle sizes of ~450 nm and low polydispersity, which can be seen by the FESEM image in Fig. 1 (a). The CPPy difficult oxidize as compared to other PPPy at different temperatures due to its bigger particles size and aggregation on the FTO surface. The detail, in Fig. 1 (b&c), shows PPPy porous film on the FTO surface decorated with small particles of diameter around 50–70 nm. The PPPy as shown in Fig. 1 (d), have uniform and porous structures and well connected networks of conducting polymer, which is a typical micro-structure for conductive polymer obtained by chemical oxidation or electrochemical polymerization method. Among the PPPy films, used of ZIF-8 gives a more porous structure and such a porous structure of PPPy may favorable for the high surface area of porous counter electrode. However, the PPPy at 120 °C has quite different morphology with non homogeneous flat crack

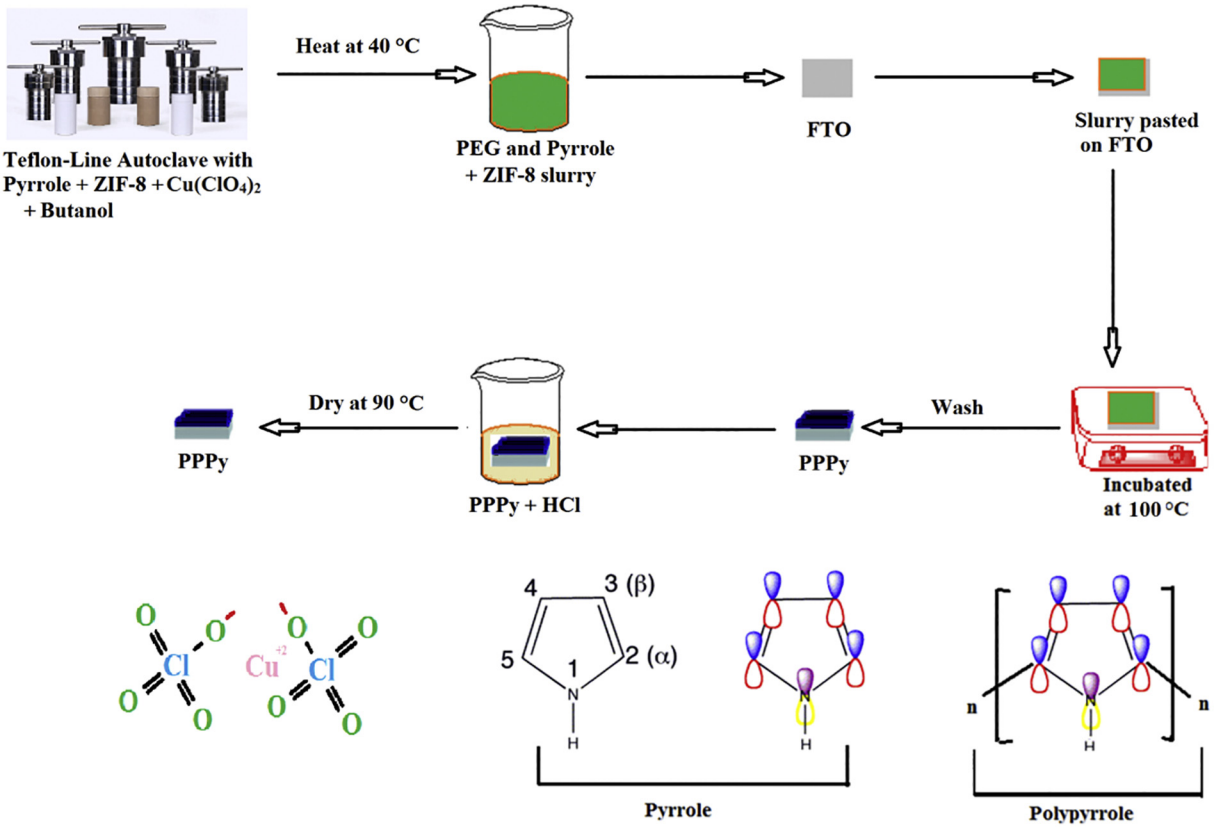

Fig. 2. Scheme of PPPy synthesis by simple hydrothermal method.

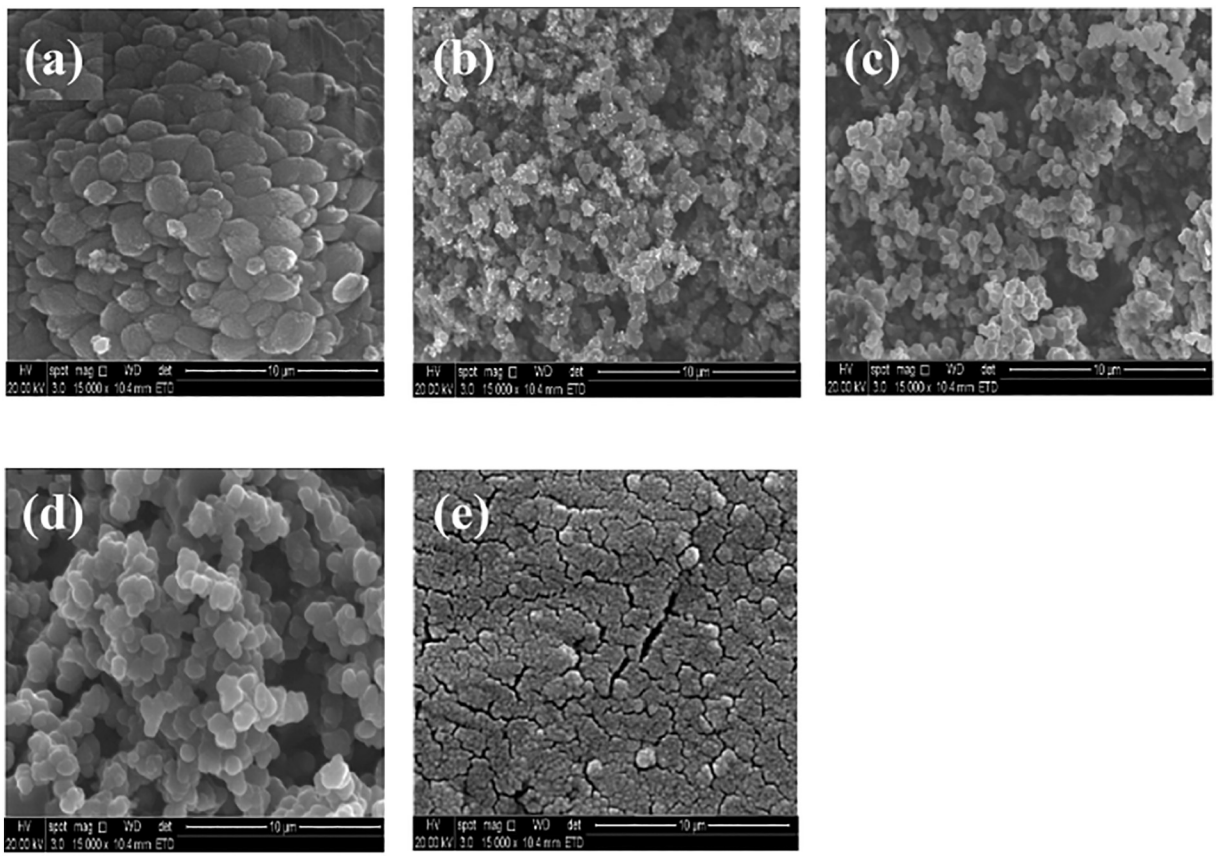

Fig. 3. FESEM images of the CPPy (a), PPPy at 60 °C (b), PPPy at 80 °C (c), PPPy at 100 °C (d), PPPy at 120 °C (e).

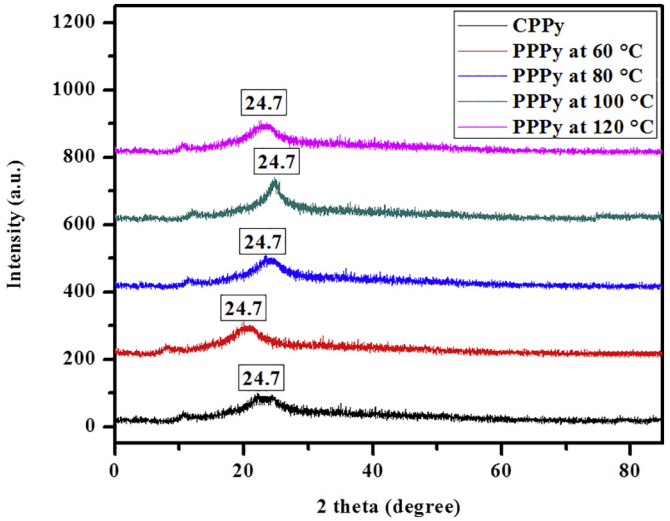

Fig. 4. XRD patterns of CPPy and PPPy at different temperatures.

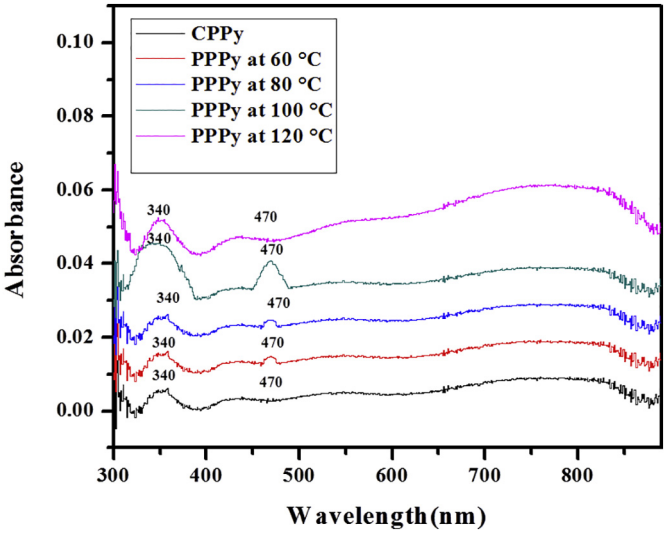

Fig. 5. UV–Vis patterns of CPPy and PPPy at different temperatures.

shaped film as sown in Fig. 1 (e), due to high temperature for polymerization.

3.2. The phase description of various counter electrodes

XRD patterns of CPPy and PPPy at different temperatures showed in Fig. 4. The CPPy and PPPy at 100 °C by simple hydrothermal method showed a broad characteristic peak at around (2θ = 24.7°) corresponding to highly disordered region, which is a proof of amorphous nature of PPy [32–34]. The PPPy at 100 °C showed broad sharp peak at around (2θ = 24.7°) due to its uniform and porous structures and well connected networks of conducting polymer, which is a typical microstructure for conductive polymer obtained by chemical oxidation. This can be attributed to scattering of PPy from all over chains. With the variation of temperatures polymerization *i.e.*, PPPy at 60 °C and PPPy at 80 °C the spectra look almost similar but peaks shifted toward lower diffraction angle and decreased intensity with comparison to the PPPy at 100 °C, respectively. These were attributed to formation of less porous structure and low level of oxidation process at low temperatures, which not improved and enhanced PPy energy conversion efficiency. Since, the hydrothermal polymerization polymer still keeps the strongest peak value, it is reasonable to believe that the polymer may keep its original main structure after hydrothermal polymerization method. The PPPy at 120 °C peak shifted toward lower diffraction angle with decreased intensity with comparison to the PPPy at 100 °C and other PPPy as more cracks and weak connected networks of conducting polymer formed on FTO surface.

3.3. Absorbance of various counter electrodes

Fig. 5, shows UV–Vis patterns of CPPy and PPPy at different temperatures. The CPPy, PPPy at 60 °C and 80 °C showed low level of oxidation and absorption shapes revealed two main peaks around wavelength 340 nm and 470 nm. It is observed that CPPy, PPPy at 60 °C and 80 °C peak intensity at wavelength 340 nm is stronger compared with that at 470 nm. The PPPy at 100 °C film show strong peak at wavelength 470 nm, which can be assigned to the transition between the valence band and the anti-bonding bipolaron band. The PPPy at 100 °C well polymerized as showed high absorbance intensity peaks at wavelength 340 nm and 470 nm after simple hydrothermal method, which is the featured typically peak in the partially doped (oxidized) state of conductive polymer and absorption at greater wavelengths is the “free carrier tail” [35,36], as compared to CPPy, PPPy at 60 °C, 80 °C and 120 °C temperatures. This featured property can be explained by the fact that the PPPy at 100 °C film is porous and high level of oxidation, firmly adhere on FTO surface due to good contact of PPPy and FTO surface. The PPPy at 120 °C absorbance intensity peaks at wavelength 340 nm and 470 nm after simple hydrothermal method were very weak due to its cracked non homogenous film. At high temperature PPPy at 120 °C results in a smoother and thicker film and noticed that only small part of film was deposited on FTO with weak peak wavelength at 470 nm.

3.4. Porous information of various counter electrodes

To further evaluate the pore properties and pores structure of ZIF-8, CPPy, and PPPy at different temperatures nitrogen absorption-desorption isothermal analysis were employed as shown in Fig. 6. A hysteresis loop exists in the range between 0.40 and 0.99 P/P^0 relative pressures between the structures of PPPy at (60 °C, 80 °C and 100 °C), presented as type IV and it indicates that the material has a mesoporous structure [37]. The hysteresis loop width increased as temperature

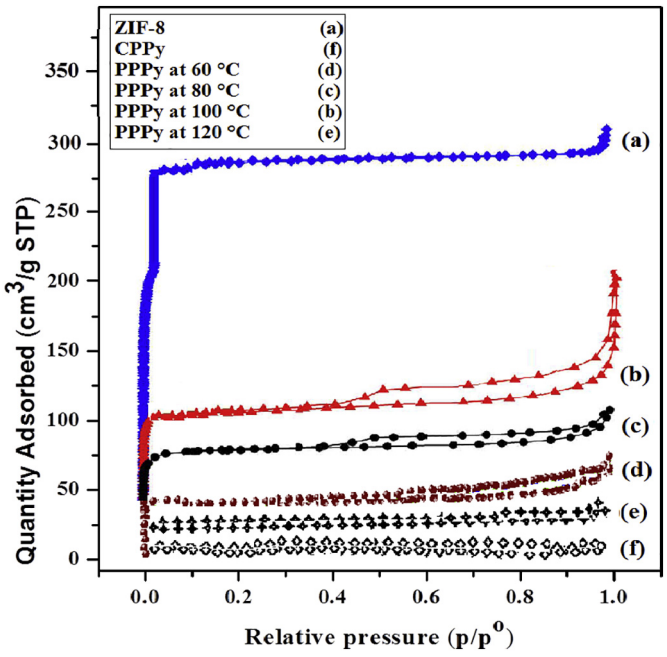

Fig. 6. BET surface area of ZIF-8, CPPy and PPPy at different temperatures.

Table 1
Detail of surface area and pore volume of ZIF-8, CPPy and PPPy at different temperatures.

Sample name	BET surface area ($m^2\ g^{-1}$)	Pore volume (cm^3/g)
ZIF-8	1080.907	0.524
CPPy	1.107	0.006
PPPy at 60 °C	125.039	0.098
PPPy at 80 °C	268.636	0.128
PPPy at 100 °C	323.12	0.197
PPPy at 120 °C	30.636	0.026

increased of PPPy from (60 °C, 80 °C and 100 °C), respectively. It can be seen that PPPy at 100 °C has a small amount of micropores and a large number of mesopores, which could enhance the electron transport between the I^-/I^{3-} redox couple and counter electrodes and show good catalytic performance. Meanwhile, at low relative pressure ($P/P^0 < 0.40$), the adsorption isotherm is rapidly saturated, indicating that it has a microporous structure [38]. The ZIF-8 displayed typical type-I behavior [39], and it reduced the catalytic performance of DSSC as compared to other PPPy. As we all know that the micropores were beneficial to the charges accumulation, while mesopores were helpful to the adsorption and transport of electrolyte ions [40–42]. Table 1 shows the specific surface area and pore volume parameters of different samples. The specific surface area and pore volume of the PPPy at 100 °C (323.12 $m^2\ g^{-1}$ and 0.197$cm^3 g^{-1}$) respectively, were bigger as compared with PPPy at (60 °C and 80 °C). While CPPy and PPPy at 120 °C catalyst exhibited decreased BET surface area due to absence of ZIF-8 and blocking of cavity windows by the deposited ZIF-8 film at high temperature, respectively. The high specific surface area and high pore volume of the material facilitate ion transfer and charge storage of the DSSC. The size of the pores affects the material's properties and therefore their suitability for use in different applications. In further research, we will focus on the development of conducting polymers with variable particle sizes and pore-size distributions, which are critical to achieving the desired performance.

3.5. Photovoltaic performance of various counter electrodes

As shown in Table 2 and Fig. 7, Pt shows the best performance among all counter electrodes, which is about 9.05%, while PPPy at 100 °C shows almost the same result 8.63% of conversion efficiency due to homogenous porous film on FTO and faster electron transport. It indicated that PPPy at 100 °C obtained through simple hydrothermal method is an excellent candidate for Pt free DSSC. However, when being treated without ZIF-8 the CPPy as CE based on DSSC device performance decrease gradually because of their lower V_{oc} and poor FF, as fill factor and V_{oc} are sensitive to interface properties (interface of FTO/polymer). The PPPy at 100 °C as CE for DSSC gave over 3.43% of efficiency than CPPy, we attribute this result to the non-homogeneous coverage of the FTO substrate during the simple hydrothermal method procedure. The PPPy at 100 °C as CE for DSSC gave over 1.45%, 0.5% and 1.91% of efficiency than PPPy at 60 °C, 80 °C and 120 °C respectively, due to the faster electron transport rate as envisaged above. Additionally, the high surface area of ZIF-8 can also ensure that the

Table 2
Cell performance of DSSC of Pt, CPPy and PPPy at different temperatures.

Counter electrodes	V_{oc}/mV	J_{sc} /mA cm^{-2}	FF	η /%
Pt	725 ± 5	17.25 ± 0.2	0.72 ± 0.01	9.05 ± 0.02
CPPy	731 ± 5	11.44 ± 0.2	0.62 ± 0.01	5.20 ± 0.02
PPPy at 60 °C	733 ± 5	14.41 ± 0.2	0.67 ± 0.01	7.18 ± 0.02
PPPy at 80 °C	749 ± 5	15.75 ± 0.2	0.69 ± 0.01	8.13 ± 0.02
PPPy at 100 °C	711 ± 5	17.03 ± 0.2	0.71 ± 0.01	8.63 ± 0.02
PPPy at 120 °C	739 ± 5	13.97 ± 0.2	0.65 ± 0.01	6.72 ± 0.02

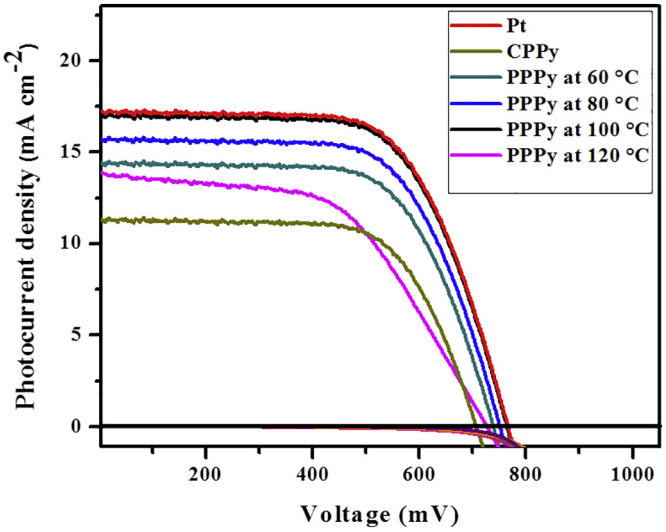

Fig. 7. J-V curves of Pt, CPPy and PPPy at different temperatures.

surface of the template metallic nanostructures is readily accessible, which is critical for the proper function of catalysts. Since, Jsc is the parameter used to evaluate the catalytic properties of the counter electrodes in our DSSC system, we believe that PPPy at 100 °C is a good candidate for use as a CE and more effort needs to be made to further improve the fill factor and such experiments are under way.

3.6. Cyclic voltammetry and catalytic behavior of PPPy at 100 °C CE

Fig. 8, shows the electrochemical behavior of PPPy at 100 °C in 0.1 M $LiClO_4$ acetonitrile solution. The PPPy at 100 °C exhibits an oxidation peak at 0.23 V with a redox peak around −0.16 V. It shows similar CV trace to those of PPy obtained from photo-electrochemical polymerization. The PPPy at 100 °C demonstrate a higher current during oxidation/reduction of the PPy thicker film and variation of peak current of the modified electrode was found to be linearly dependent on scan rate, indicating an electro-active surface bound species.

As shown in Fig. 9, two typical I^-/I_3^- redox reaction peaks were observed when Pt and PPPy at 100 °C were used as the working electrodes in the range of −1.0-1.5 V. The PPPy at 100 °C film shows very similar catalytic behavior for the redox of I^-/I_3^- to Pt, then it could be

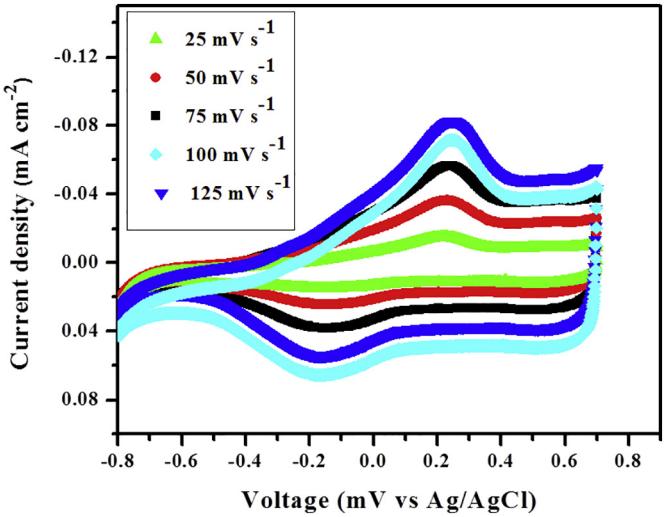

Fig. 8. CV curves of PPPy at 100 °C in 0.1 M $LiClO_4$ acetonitrile solution at various scan rates.

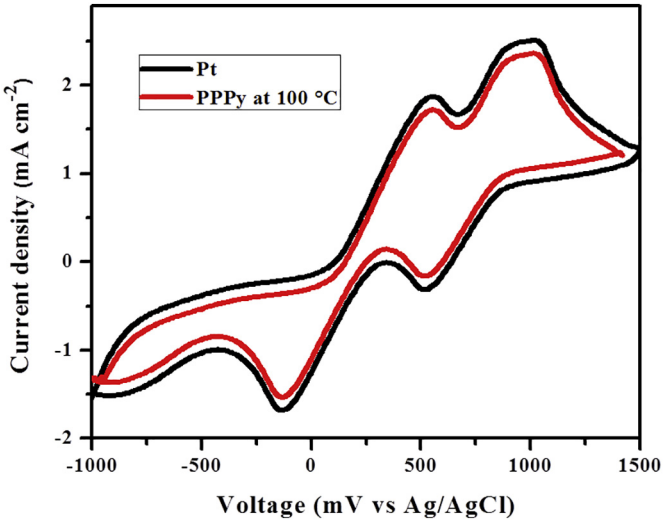

Fig. 9. Cyclic voltammograms of iodine species of Pt and PPPy at 100 °C CEs in acetonitrile solution of 10 mM LiI, 1 mM I_2 and 0.1 M $LiClO_4$.

confirmed that PPPy at 100 °C obtained by simple hydrothermal polymerization could enhance the electron transport between I^-/I_3^- redox couple and counter electrodes of conductive polymer may take part in electrochemical reaction [43,44]. The PPPy at 100 °C by simple hydrothermal polymerization, it seems that ZIF-8, serving as template, is not effect because no additional peak in the scan range during electrochemistry measurement. Therefore, ZIF-8 is stabilized in polymer chain and will not be released or be captured under the scanning range between −1 V and 1.5 V. Therefore ZIF-8 is an active stabilized in polymer chain species from viewpoint of electrochemistry by simple hydrothermal polymerization is a good means for the preparation of porous polymers when taking DSSC device operating condition into consideration.

3.7. Electrochemical impedance of Pt and PPPy at 100 °C

As shown in Fig. 10, two semicircles were observed in the measured frequency range from 10^{-1} to 10^5 Hz for all devices and the results are based on the equivalent circuits [45–47] shown as an inset in the Figure. According to the previous works [45], the semicircles in the frequency regions 10^3–10^5 and 1–10^3 Hz correspond to charge-transfer processes occurring at the counter electrode/electrolyte (R_1) and the

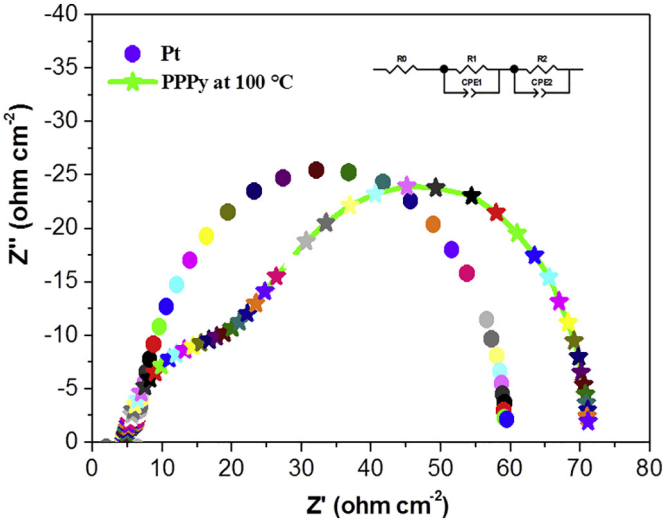

Fig. 10. Electrochemical impedance spectra of Pt and PPPy at 100 °C.

Table 3
Parameters obtained by fitting the impedance spectra of DSSC of Pt and PPPy at 100 °C.

Compounds	R_0 Ω cm^2	R_1 Ω cm^2	R_2 Ω cm^2
Pt	4.30	2.60	52.68
PPPy at 100 °C	4.60	18.38	48.23

TiO_2/dye/electrolyte interface (R_2). After PPPy at 100 °C replaces Pt electrode, R_1 increased a lot to 18.38 Ω cm^2 compared with 2.60 Ω cm^2 of Pt while R_2 drops a little bit from 48.23 Ω cm^2 to 52.68 Ω cm^2 (Table 3). The ZIF-8 is partially intercalated into the polymer structure that causes porous structure of polymer and causes adhesion of polymer and FTO surface, which increases flow of charge-transfer for current flow. The study shows that interface between FTO and conductive polymer has great impact on R_1. Therefore, better performance would be expected when we further improve the contact between PPPy at 100 °C and FTO substrate. Due to large surface area, it is expected that ZIF-8 nano-particles yield better contact with polymer matrix.

4. Conclusions

In summary, PPPy was synthesized, used ZIF-8 as template by simple hydrothermal method and employed as counter electrode in DSSC. The ZIF-8 increased the surface area and pore volume of PPPy at 100 °C in comparison with other polymers obtained after simple hydrothermal method were high, as determined by NOVA 4200e Surface Area & Pore Size Analyzer. The analyses were consistent with a structure that ZIF-8 is partially intercalated into the polymer structure. Electrochemical and photo-electrochemical as well as impedance spectra measurements revealed that ZIF-8 as template by the simple hydrothermal method polymerization is a effective way for preparing PPPy (CE) in DSSC, which may open up an alternative choice for the future industrial application. In DSSC, PPPy at 100 °C is one of the most promising material used for nano-porous thin film when, it serves as counter electrode due to its appropriate low cost, and easy preparation. However, traditional preparation methods are involved in expensive equipment, complicated process and high production cost.

Acknowledgment

This work was supported by the National Natural Science Foundation of China (NSFC 51402111 and 21528301), and the Fundamental Research Funds for the Central Universities (SCUT Grant No. 2018ZD21).

Author statement

We would like to submit the enclosed manuscript entitled “Increased Power Conversion Efficiency of Dye-Sensitized Solar Cells with Counter Electrodes based on Porous Polypyrrole” for your consideration for publication as an “Original Article” Reactive and Functional Polymers. This paper is new neither the entire paper nor any part of its content has been published or has been accepted elsewhere. It is not being submitted to any other journal.

We read and have abided by the statement of ethical standards for manuscripts submitted to “Reactive and Functional Polymers”. Thanks very much for your attention to our paper. Correspondence and phone calls about the article should be addressed to Shahzad Ahmad Khan at the following address, phone and email address:

Guangzhou Key Laboratory for Surface Chemistry of Energy Materials, New Energy Research Institute, College of Environment and Energy, South China University of Technology, Guangzhou, China.

Declration of Competing Interest

We would like to submit the enclosed manuscript entitled "Increased Power Conversion Efficiency of Dye-Sensitized Solar Cells with Counter Electrodes based on Porous Polypyrrole" for your consideration for publication as an "Original Article" Reactive and Functional Polymers. The porous polypyrrole (PPPy) was synthesized with zeolitic imidazolate framework-8 (ZIF-8) used as template by simple hydrothermal. The resultant PPPy was employed as counter electrode (CE) in dye-sensitized solar cell (DSSC). The 5% $Cu(ClO_4)_2$ and 2% ZIF-8 ratio in PPPy at 100 ˚C by simple hydrothermal method demonstrates comparable performance with traditional Pt in DSSC as CE, which may open up an alternative choice for the future industrial application.

References

[1] B. O'Regan, M. Gratzel, Nature 353 (1991) 737.
[2] A. Kay, M. Gratzel, Sol. Energy Mater. Sol. Cells 44 (1996) 99.
[3] T.N. Murakami, S. Ito, Q. Wang, M.K. Nazeeruddin, T. Bessho, I. Cesar, P. Liska, R.H. Baker, P. Comte, P. Pechy, M. Gratzel, J. Electrochem. Soc. 153 (2006) A2255.
[4] M. Wu, X. Lin, T. Wang, J. Qiu, T. Ma, Energy Environ. Sci. 4 (2011) 2308.
[5] S.I. Cha, B.K. Koo, S.H. Seo, D.Y. Lee, J. Mater. Chem. 20 (2010) 659.
[6] T. Denaro, V. Baglio, M. Girolamo, V. Antonucci, A.S. Arico, F. Matteucci, R. Ornelas, J. Appl. Electrochem. 39 (2009) 2173.
[7] J. Han, H. Kim, D.Y. Kim, S.M. Jo, S.Y. Jang, ACS Nano 4 (2010) 3503.
[8] S. Sakurai, H. Jiang, M. Takahashi, K. Kobayashi, Electrochim. Acta 54 (2009) 5463.
[9] K.M. Lee, W.H. Chiu, H.Y. Wei, C.W. Hu, V. Suryanarayanan, W.F. Hsieh, K.C. Ho, Thin Solid Films 518 (2010) 1716.
[10] K.M. Lee, P.Y. Chen, C.Y. Hsu, J.H. Huang, W.H. Ho, H.C. Chen, K.C. Ho, J. Power Sources 188 (2009) 313.
[11] S. Ameen, M.S. Akhtar, Y.S. Kim, O.B. Yang, H.S. Shin, J. Phys. Chem. C 114 (2010) 4760.
[12] H. Nagai, H. Segawa, Chem. Commun. 8 (2004) 974.
[13] J. Wu, Q. Li, L. Fan, Z. Lan, P. Li, J. Lin, S. Hao, J. Power Sources 181 (2008) 172.
[14] M. Wu, X. Lin, A. Hagfeldt, T. Ma, Angew. Chem. Int. Ed. 50 (2011) 3520.
[15] M. Wu, X. Lin, Y. Wang, L. Wang, W. Guo, D. Qi, X. Peng, A. Hagfeldt, M. Gratzel, T. Ma, J. Am. Chem. Soc. 134 (2012) 3419.
[16] Q.W. Jiang, G.R. Li, X.P. Gao, Chem. Commun. 44 (2009) 6720.
[17] Y. Hu, Z. Zheng, H. Jia, Y. Tang, L. Zhang, J. Phys. Chem. C 112 (2008) 13037.
[18] M. Wang, A.M. Anghel, B. Marsan, N.L. Cevey, N. Pootrakulchote, S.M. Zakeeruddin, M. Gratzel, J. Am. Chem. Soc. 131 (2009) 15976.
[19] H. Sun, D. Qin, S. Huang, X. Guo, D. Li, Y. Luo, Q. Meng, Energy Environ. Sci. 4 (2011) 2630.
[20] R. Balint, N.J. Cassidy, S.H. Cartmell, Acta Biomater. 10 (2014) 2341.
[21] D.N. Nguyen, H. Yoon, Polymers. 8 (2016) 118.
[22] E.Z. Mohd Tarmizi, H. Baqiah, Z.A. Talib, J. Solid State Electrochem. 21 (2017) 3247.
[23] S.S. Shinde, G.S. Gund, D.P. Dubal, S.B. Jambure, C.D. Lokhande, Electrochim. Acta 119 (2014) 1.
[24] A. Batool, F. Kanwal, M. Imran, T. Jamil, S.A. Siddiqi, Synth. Met. 161 (2011) 2753.
[25] J. Tabačiarova, M. Mičušik, P. Fedorko, M. Omastova, Polym. Degrad. Stab. 120 (2015) 392.
[26] Yu Kai, Kumar Narendra, Roine Jorma, Ivaska Ari, RSC Adv. (62) (2014) 33120.
[27] M. Jaymand, RSC Adv. 64 (2014) 33935.
[28] A. Rashidzadeh, A. Olad, S. Ahmadi, Polym. Eng. Sci. 53 (2013) 970.
[29] M.A. Hussein, B.M. Abu-Zied, A.M. Asiri, Polym. Compos. 36 (2014) 1160.
[30] A.C. Lopes, P. Martins, S. Lanceros-Mendez, Prog. Surf. Sci. 89 (2014) 239.
[31] J. Cravillon, S. Munzer, S.J. Lohmeier, A. Feldhoff, K. Huber, M. Wiebcke, Chem. Mater. 21 (2009) 1410.
[32] P. Mavinakuli, S. Wei, Q. Wang, A.B. Karki, S. Dhage, Z. Wang, D.P. Young, Z. Guo, J. Phys. Chem. C 114 (2010) 3874.
[33] J. Hazarika, A. Kumar, Synth. Met. 175 (2013) 155.
[34] J.Chan drasekara, optic 124 (2013) 2057.
[35] Y. Xia, A.G. MacDiarmid, A.J. Epstein, Macromolecules. 27 (1994) 7212.
[36] D. Hohnholz, A.G. MacDiarmid, D.M. Sarno, W.E. Jones, Chem. Commun. (23) (2001) 2444.
[37] Y. Zhang, H. Jiang, Q. Wang, J. Zheng, C. Meng, Appl. Surf. Sci. 447 (2018) 876.
[38] Z. Liu, Z. Zhu, J. Dai, Y. Yan, Chemistryselect. 3 (2018) 5726.
[39] Y. Zhao, et al., Catal. Commun. 57 (2014) 119.
[40] G. Zhang, Y. Chen, Y. Chen, H. Guo, Mater. Res. Bull. 102 (2018) 391.
[41] J. Pang, W. Zhang, H. Zhang, J. Zhang, H. Zhang, G. Cao, M. Han, Y. Yang, Carbon. 132 (2018) 280.
[42] J. Wei, S. Wan, P. Zhang, H. Ding, X. Chen, H. Xiong, S. Gao, X. Wei, New J. Chem. 42 (2018) 6763.
[43] T. Yohannes, O. Inganäs, Sol. Energy Mater. Sol. Cells 51 (1998) 193.
[44] S. Biallozor, A. Kupniewska, Electrochem. Commun. 2 (2000) 480.
[45] L. Han, N. Koide, Y. Chiba, T. Mitate, Appl. Phys. Lett. 84 (2004) 2433.
[46] Q. Wang, J.E. Moser, M. Grätzel, J. Phys. Chem. B 109 (2005) 14945.
[47] J. Tornow, K. Schwarzburg, J. Phys. Chem. C 111 (2007) 8692.